

# **PACIFIC HINDCAST PERFORMANCE EVALUATION OF THREE NUMERICAL WAVE MODELS**

**Jeffrey L. Hanson**

US Army Corps of Engineers  
Field Research Facility, Duck, NC  
Email: Jeffrey.L.Hanson@erdc.usace.army.mil

**Barbara A. Tracy**

US Army Corps of Engineers, Waterways Experiment Station, Vicksburg, MS

**Hendrik L. Tolman**

SAIC-GSO, Environmental Modeling Center NOAA-NCEP Camp Springs, MD

**R. Douglas Scott**

W.F. Baird & Associates Coastal Engineers, Ottawa, Ontario, Canada

## **1. INTRODUCTION**

The US Army Corps of Engineers (USACE) Wave Information Study (WIS) program (Tracy and Cialone, 2004) is establishing a multi-decade wave climatology for the Pacific basin to support a variety of coastal planning and engineering activities. To facilitate selection of an appropriate wave hindcast technology, the performance of three modern numerical spectral wave models is evaluated in the Pacific basin over calendar year 2000. The technologies evaluated include the third-generation wave model WAM Cycle 4.5 (Gunther, 2002), the third-generation wave model WAVEWATCH III (Tolman 1997, 1999, 2002a), and the second-generation wave model WAVAD (Resio and Perrie, 1989).

A significant challenge in evaluating basin-scale wave hindcasts is the need to reduce statistically millions of spectral estimates to a meaningful measure of performance yet retain sufficient level of detail to provide useful guidance on model strengths and deficiencies. Rather than rely solely on the limited amounts of information contained in integral or 'bulk' wave statistics (see for example Cardone et al. 1996, Hsu et al. 2002, O'Reilly et al. 1996, and Tolman 2002b), we employ here a wave systems approach for assessing the performance of each model hindcast. This approach is based on wave spectral partitioning methods of Hanson and Phillips (2001) and extends the model evaluation and diagnostic methods reported by Hanson and Jensen (2004), herein referred to as HJ04.

Using buoy data as ground truth, HJ04 assessed hindcast skill by determining how well a model correctly represented the spectral signatures of individual wind sea and swell wave systems passing through each buoy location. Here we extend that approach with improved metrics for directional data, a quantile-quantile statistical analysis of events, and a novel scoring technique using normalized performance indicators with sample size weighting factors. The results provide both a convenient account of model skill in

representing the heights, periods and directions of the various wind sea, young swell and mature swell wave systems, and provide a distinctive diagnostic capability to identify model deficiencies.

Each of three modeling technologies was used to generate a full Pacific basin hindcast (110° E to 60° W; 64° S to 64° N) using identical wind fields over the calendar year 2000. Model validations were conducted at seven disparate deep water buoy sites. The results provide a distinctive view of model performance and facilitated selection of a hindcast technology for the WIS multi-decade study.

## 2. WAVE MODEL HINDCASTS

A fundamental issue addressed early in this investigation was how much to restrict individual model runs to identical computational environments, boundary conditions, grid resolution, source term parameter settings, etc. As the purpose of this investigation was to identify the best performing technology for the WIS Pacific hindcast, and not strictly to compare the details of model technologies, we adopted a relaxed set of guidelines for performing the hindcasts. An overview of the resulting hindcast runs appears in Table 1. Each group of modelers was allowed to select a bathymetry grid and develop model set up parameters to optimize individual model performance in their own computing environment. However, for all model runs, they used a common set of high-quality wind fields that spanned the entire Pacific Ocean basin for the full calendar year 2000. To further limit analysis-induced bias, all buoy data validations were performed using the same observation sets with a fixed frequency range and angular resolution. Specific details on the wind fields and model hindcast runs appear in the following sections.

**Table 1.**  
**Wave Model Hindcast Runs**

<b>Hindcast Technology</b>	<b>Primary Contact(s)</b>	<b>Run Date</b>	<b>Computational Environment</b>	<b>Bathymetry</b>	<b>Grid Resolution</b>	<b>Wind Forcing</b>
WAM	R. Jensen (USACE)	12 OCT 2005	Cray X1 Single Processor	GEBCO* with Obstructions	0.5 x 0.5 deg	Oceanweather NRAQ
WAVEWATCH III version 2.22	H. Tolman (NCEP) B. Tracy (USACE)	23 SEP 2005	Origin O3K Parallel Processor Using MPI	NOAA Grid with Obstructions (from etopo2)	0.5 x 0.5 deg	Oceanweather NRAQ
WAVAD	D. Scott (Baird)	21 OCT 2005	3.4 GHz Personal Computer	NOAA Grid with Obstructions (from etopo2)	0.5 x 0.5 deg	Oceanweather NRAQ

\*General Bathymetric Chart of the Oceans, <http://www.gebco.net>

## 2.1 Wind Fields

A high-quality, consistent set of wind fields are being developed for WIS with the goal of accurately representing the full range of meteorological events that occur in the Pacific. These wind fields are generated by the marine meteorology group at Oceanweather, Inc. (OWI) using baseline National Centers for Environmental Prediction-National Center for Atmospheric Research (NCEP-NCAR) global reanalysis (NRA) 6-hourly, 10-m surface winds on a Gaussian geographic grid (Kalnay et al. 1996). The NRA fields are adjusted using QuickSCAT (Q/S) scatterometer winds by linear regressions through quantile-quantile (QQ) plots in 45-deg wind direction sectors grouped north of the equator in six 10-degree latitude bins from about 180-deg W to just off the North American west coast. Wind field estimates west of 180-deg W mirror the eastern corrections and extend to the Asian coast. Southern hemisphere points are not adjusted. A three-grid-point buffer between adjustments at coastal points and at zonal boundaries is used to blend regions. Additional coastal corrections are made point by point. Wind direction bias is removed using mean sector differences. NRA data from the full year (2000) are included in the QQ analysis, as seasonally stratified regressions are not statistically independent. Beyond the Q/S adjustments, no additional observations are used in the analysis of the NRA-QuickSCAT winds. Furthermore, tropical cyclone winds from the OWI mesoscale Planetary Boundary Layer (PBL) cyclone model are blended in. The resulting wind fields, called NRAQ+, are interpolated at 3-hour intervals on a 0.5-degree spatial hindcast grid. Compared to the NRA winds, the NRAQ+ winds are superior in capturing synoptic and meso-scale events.

In addition to the NRAQ+ results, a third level of analysis can also be performed using manual kinematic techniques for top ranked storms in each geographic region (Cox et. al. 1996). All available buoy data are included in the Level III analysis (Cox and Cardone, 2000). A 1-month set of NRAQ+ winds were generated to assess the impact of higher quality winds on hindcast performance.

## 2.2 Wave Models

Numerical wave models solve the action balance equation:

$$\frac{\partial N}{\partial t} + \vec{C}_g \cdot \nabla N = \sum_{i=1}^n S_i ,$$

where the action density  $N = S(\omega, \theta) / \omega$ ,  $S(\omega, \theta)$  is the energy-frequency spectrum, radian frequency  $\omega = 2\pi f$ , and  $\vec{C}_g$  is the vector wave group velocity. The source terms on the right hand side are given by

$$S_{total} = S_{in} + S_{nl} + S_{ds} ,$$

with source mechanisms grouped into a wind input term ( $S_{in}$ ), nonlinear wave-wave interaction term ( $S_{nl}$ ), and dissipation term ( $S_{ds}$ ). The momentum transferred to waves

and currents by the winds is captured by  $S_{in}$ . The spectral exchange of energy between frequencies is described by  $S_{nl}$ . For open ocean deep-water wave propagation, the primary  $S_{ds}$  mechanism is wave breaking.

Here we compare results from three wave models: WAM, WAVEWATCH III and WAVAD. Each model defines directional spectra in terms of 25 logarithmically spaced frequency bins and 24 regularly spaced direction bins of 15-deg width. For the model validation analysis, the two lowest frequency bins were dropped from the analysis in order to match the frequency range of the ground-truth buoy data. The models were initiated on 1 January 2000 and run for a full calendar year. The first two weeks of ‘spin-up’ in January were excluded from the analysis.

### *WAM Model*

In the third generation WAM Cycle 4.5 (Komen et al. 1994; Gunther, 2002), all source terms are specified with degrees of freedom equal to those of resulting directional wave spectra, with no *a-priori* assumptions regarding spectral shapes. WAM solves the action balance equation in two parts: (a) propagation of energy on a fixed grid, and (b) the temporal change of action that is effected by the source terms. Internal time steps and output resolution control model run times in time and space.

For this study, a 12-month WAM Pacific hindcast was produced using the NRAQ+ winds for year 2000. The latest version of WAM (Cycle 4.5) was run on a Cray X1 platform with no parallelization (Table 1). The modeling domain consisted of 19,127 active water points at 0.5-deg spatial resolution covering 64 S to 64 N Latitude and 110 E to 60 W Longitude. Water depths were obtained from General Bathymetric Chart of the Oceans (GEBCO), a digital bathymetry database with nominal horizontal resolution of 3-minutes. Depth data were then sub-sampled to a 0.5-deg fixed longitude, latitude grid, and edited to include spatially unresolved islands. A 1200-s internal time step was used for all calculations, with output exported hourly. Full directional wave spectra were saved at 23 points, corresponding to the locations of available Pacific wave buoys (1D and 2D), including the buoys used in this study.

### *WAVEWATCH III*

The third-generation numerical wave model WAVEWATCH III Version 2.22 (Tolman, 2002a) was developed at the NOAA National Centers for Environmental Prediction (NCEP), Marine Modeling and Analysis Branch, and is used by NOAA for operational numerical wave simulations. Structurally very similar to WAM, WAVEWATCH III was run with the standard operational default settings that include the Tolman and Chalikov (1996) source functions. The operational basin-level Pacific grid was 64 S to 64 N Latitude and 110 E to 60 W Longitude with 0.5-deg spatial resolution. A 0.5-deg resolution obstruction grid was used to simulate wave blocking by the Pacific Islands.

As with WAM, a 12-month Pacific hindcast was produced using the NRAQ+ winds for the year 2000. WAVEWATCH III version (2.22) was run on an Origin O3K platform in MPI parallel mode using 16 processors (Table 1). WAVEWATCH III requires four input time steps. The global time step that propagates the entire solution in time for the basin level run was set to 3600 sec. The spatial propagation time step was set to 1100 sec. The third time step that relates to refraction effects for shallow water grids was set to 3600 sec, and the final time step for integration of the source terms was set to 150 sec to allow for quickly changing wind and wave conditions. Hourly wave parameter and directional wave spectra were saved at each of the ground truth stations used by this study.

### WAVAD

The second generation (2G) spectral wave model WAVAD (Resio and Perrie, 1989) calculates directional wave spectra and related wave characteristics over a given spatial domain on the basis of input winds and bottom bathymetry. As a 2G model, WAVAD maintains equilibrium between the input winds and the non-linear wave energy flux with an assumed  $f^{-4}$  spectral shape. Wave growth is based on a combined Phillips and Miles mechanism. Weak non-linear wave-wave interactions are represented as a momentum flux to both lower and higher frequencies away from the spectral peak. Energy transferred to higher frequencies is assumed to be lost by breaking. Wave propagation in the model is achieved by means of a semi-Lagrangian first-order approach.

The WAVAD hindcasts were produced on a 3.4 GHz personal computer using the identical bathymetry and obstruction grids used for WAVEWATCH III. As with the other models, a 12-month Pacific hindcast was produced using the NRAQ+ winds for 2000. Spectral output was archived at hourly intervals for the selected buoy locations, and wave parameter fields over the entire grid were saved at 6-hourly intervals. A time step of 1800 seconds was utilized in the model.

### 3. OBSERVATIONS

The wave system validation method requires both wind observations and either directional (2D) or non-directional (1D) wave spectra as input. Ground truth data were obtained from the National Buoy Data Center (NDBC) and Coastal Data Information Program (CDIP) buoy networks. The seven deep-water wave stations used in this study are shown on Figure 1. These stations cover offshore conditions for much of the US and are sufficiently well dispersed to include a wide range of wave generation and swell propagation environments. Specific details on these stations appear in Table 2. Included are a variety of measurement platforms and instrumentation types, including three stations equipped with directional wave sensors (46042, 071 and 51028).

The meteorological data from the NDBC stations include hourly 8-min average wind speed and direction at a sensor height of 5-m above sea level. Measurement accuracy is  $\pm 1.0$  m/s for wind speed and  $\pm 10$  degrees for wind direction. Although there is no wind sensor at CDIP station 071, we adopt here the successful approach of HJ04 and use the

winds from NDBC station 46063, located 23 km southeast of 071, to estimate local wind-generated forcing around CDIP station 071.

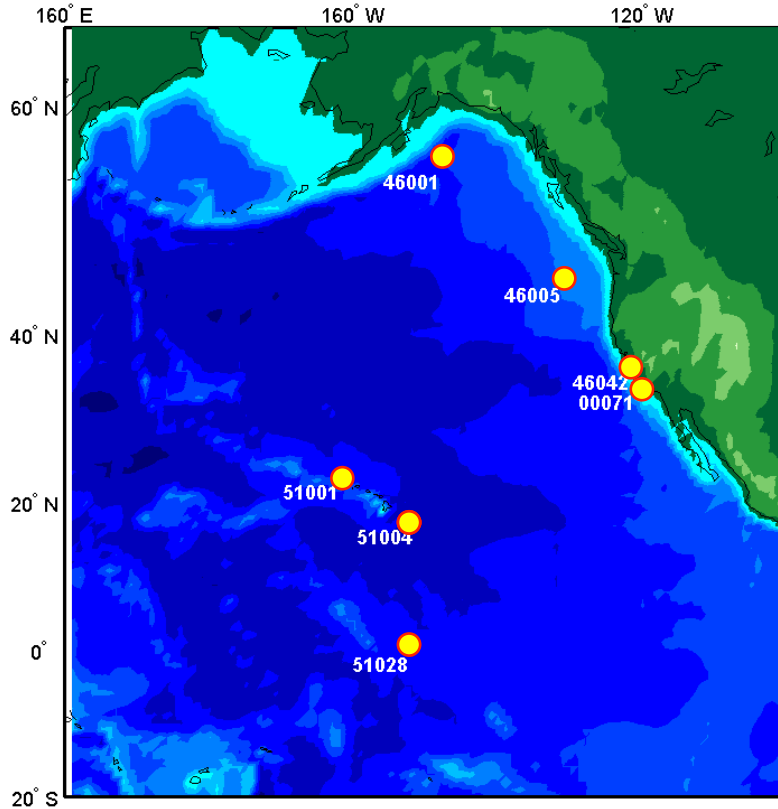


Figure 1. Pacific Hindcast Validation Stations

Processing of directional wave spectra is as reported by HJ04. Wave spectra from the NDBC stations were computed hourly from 20-minute records for frequencies ranging from 0.03 to 0.4 Hz. The CDIP directional wave data were computed from half-hour records over the frequency band 0.025 – 0.58 Hz. For the three directional wave buoys, the maximum-likelihood estimator of Oltman-Shay and Guza (1984) was used to compute the directional wave spectrum  $S(f, \theta)$  from the NDBC and CDIP spectral parameters. The resulting spectra were linearly interpolated to the 23-frequency (.04 Hz to .34 Hz), 15-deg bin resolution used for this analysis. Non-directional spectra were interpolated in frequency only. As will be shown, these interpolations are necessary to make one-to-one comparisons between buoy and hindcast spectral features.

**Table 2.**  
**Observation Stations**

<b>Organization</b>	<b>Station ID</b>	<b>Platform</b>	<b>Payload</b>	<b>Data Used</b>	<b>Depth (m)</b>	<b>Latitude N</b>	<b>Longitude W</b>	<b>Location</b>
NDBC	46001	6-meter NOMAD	ARES 4.4	Met, 1D Waves	4206	56°17'44"	148°10'19"	Gulf of Alaska
NDBC	46005	6-meter NOMAD	ARES	Met, 1D Waves	2780	46°03'00"	131°01'12"	Aberdeen, WA
NDBC	46042	3-m discus	DACT	Met, 2D Waves	1920	36°45'11"	122° 25'21"	Monterey, CA
CDIP	071	0.9-m sphere	Datawell MK II	2D Waves	549	34°27'02"	120°46'07"	Harvest, CA
NDBC	51001	3-m discus	ARES	Met, 1D Waves	3252	23°25'55"	162°12'28"	Northwest Hawaii
NDBC	51004	3-m discus	ARES	Met, 1D Waves	5303	17°31'21"	152°28'51"	Southeast Hawaii
NDBC	51028	3-m discus	ARES	Met, 2D Waves	4755	00°01'12"	153°52'12"	Christmas Island

#### 4. PERFORMANCE EVALUATION METHOD

The validation of wave model output at the wave system level requires an efficient approach to characterize energy levels of individual wind-sea and swell wave components in directional wave spectra. As Figure 2 depicts, a ‘wave component’ is defined as a specific wind-sea or swell that can be attributed to a region of enhanced energy in a directional wave spectrum. The evolution of a series of related wave components forms a ‘wave system.’ Hence a wave system is considered to be the total set of waves propagating from a specific storm or generation region on the ocean surface. A unique wave model evaluation approach was developed in support of the WIS and MOdeling the Relevant PHysics Of Sedimentation in 3D (MORPHOS-3D) programs. Called the Wave Model Evaluation and Diagnostics System (WaveMEDS), the method uses wave component and wave system attributes of evolving wave spectra to quantify model skill across a variety of metrics, fold these metrics into overall measures of performance, and diagnose model deficiencies. The specific analysis steps in WaveMEDS are outlined in the following sections.

##### 4.1 Wave Partitioning

A spectral partitioning method (Hanson and Phillips, 2001, herein referred to as HP01) is employed to identify the wave components and systems at each ground truth station (Table 1). Spectral partitioning allows the identification of components and grouping of wave systems from spatially and temporally distributed observations of directional wave

spectra. The frequency and direction domains associated with each dominant peak in a wave spectrum form a spectral partition that is associated with that particular wave component (Figure 2a). For each spectrum, a unique partition template is formed that identifies the boundaries between adjacent wave components. We employ the improvements to this method as reported by HJ04, including the use of efficient image processing routines in the partitioning algorithm. Furthermore, we have now extended the method of HP01 to allow for the partitioning of non-directional (1D) spectral data.

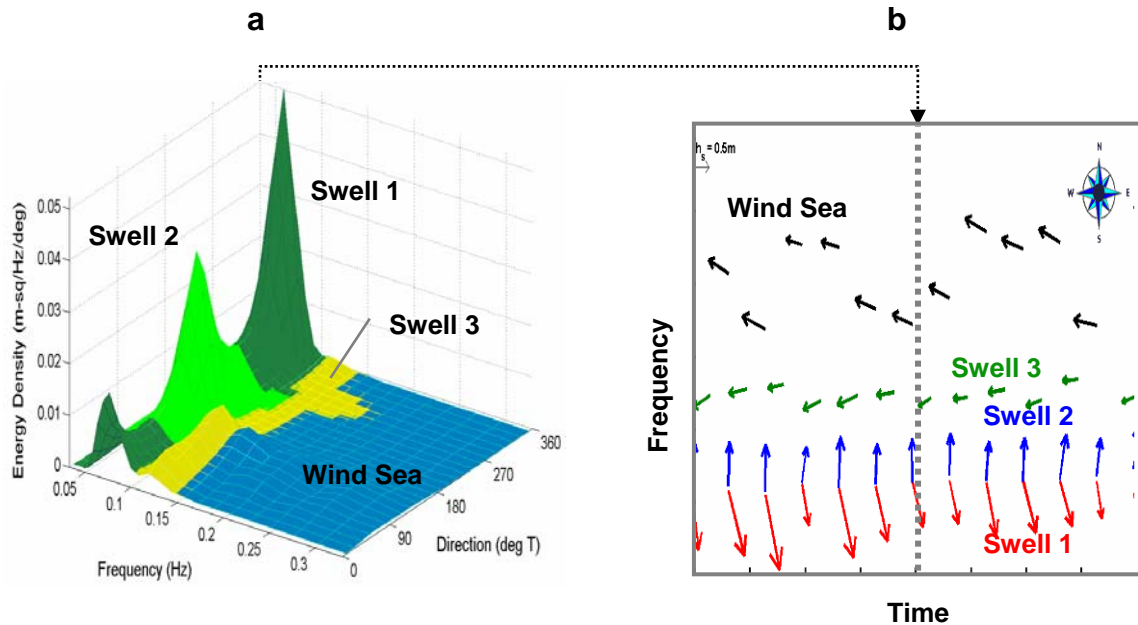


Figure 2. Sample wave features showing (a) spectral components and (b) wave system evolution. In (b), the height, peak frequency and mean direction of propagation are represented by vector length, origin and azimuth, respectively.

As reported in HJ04, a variety of physical attributes are computed for each wave component, including the significant wave height ( $H_s$ ) and peak period ( $T_p$ ). For directional data, the mean direction ( $\bar{\theta}$ ) and directional spread ( $\sigma$ ) are also computed. The isolated wave components at each station are divided into three wave maturity classes: wind sea, young swell, and mature swell. The HP01 wave age criterion is used to classify spectral peaks that are forced by the local wind as wind sea. Remaining wave components that have a peak frequency of 0.09 Hz or greater are classified as young swell, and those with a peak frequency less than 0.09 Hz are classified as mature swell. This frequency division was found to be a somewhat natural separation between regionally-generated young swell and swell that has traveled significant distances in the Pacific. Cluster algorithms allow the tracking of wave systems through time (Figure 2b). Thus, rather than describe each wave spectrum by a single set of bulk or integral

quantities, each spectrum is characterized by the  $H_s$ ,  $T_p$ ,  $\bar{\theta}$  and  $\sigma$  attributes for the individual wind sea and swell systems present.

## 4.2 Wave Component Statistics

In this step, we evaluate the wave hindcast differences from observations for each wind-sea and swell component extracted from the buoy data. These differences are attributed to model errors, which makes the assumption that buoy data are truth. As described in HJ04, each hourly hindcast spectrum is time paired to the corresponding buoy spectrum for that location. Time lags of up to 10 min between hindcast and buoy times are allowed. For each wave component, the buoy partition template (see above) is used to identify the corresponding spectral domain in the hindcast spectra. A matching set of hindcast attributes ( $H_s$ ,  $T_p$ ,  $\bar{\theta}$  and  $\sigma$ ) are computed and paired with the appropriate buoy quantities, resulting in a unique set of paired wave component attributes for each model run.

At each station, the hindcast wave component attributes are evaluated against the observed quantities using monthly temporal correlation (TC) analyses and quantile-quantile (QQ) distributions in 99 percentile bins. The TC analysis provides an indication of how well the hindcast quantities match the observed quantities in absolute time. For example, a time offset in identical hindcast magnitudes would degrade the TC results. In contrast, the QQ analysis is used to indicate if the distribution of parameter magnitudes is correct, regardless of occurrence time. For an assessment of engineering loading, a correct time sequence may not be as important as having a proper distribution. The TC comparisons were performed on the height, period, direction and spread attributes and the QQ distributions were performed on the height and period attributes. These analyses were performed on the monthly data records at each station.

A variety of established metrics are used to quantify the TC and QQ comparisons. For the series of buoy measurements  $m$  and hindcasts  $h$  these metrics include the bias (hindcast-buoy)

$$b = \frac{1}{n} \sum h - m ;$$

root-mean-square (RMS) error

$$E_{RMS} = \left[ \frac{\sum (h - m)^2}{n} \right]^{0.5} ;$$

scatter index

$$SI = \frac{\sigma_d}{\bar{m}},$$

where the standard deviation of difference is given by

$$\sigma_d = \left[ \frac{\sum_i (h_i - m_i - b)^2}{n-1} \right]^{0.5}$$

(Cardone et al. 1996), and for directional data, angular bias (Bowers et. al. 2000)

$$b_a = \left\{ \begin{array}{ll} \tan^{-1}\left(\frac{S}{C}\right), & S > 0, C > 0 \\ \tan^{-1}\left(\frac{S}{C}\right) + \pi, & C < 0 \\ \tan^{-1}\left(\frac{S}{C}\right) + 2\pi, & S < 0, C > 0 \end{array} \right\},$$

where S and C are computed from the directional differences  $\Delta\theta = |\theta_h - \theta_m|$  by

$$S = \sum_{i=1}^n \sin(\Delta\theta_i)$$

$$C = \sum_{i=1}^n \cos(\Delta\theta_i)$$

and the circular correlation (Tracy, 2002)

$$cor = \frac{\sum_{i=1}^n \sin(\theta_m - \bar{\theta}_m) \sin(\theta_h - \bar{\theta}_h)}{\sqrt{\sum_{i=1}^n (\sin(\theta_m - \bar{\theta}_m))^2 \sum_{i=1}^n (\sin(\theta_h - \bar{\theta}_h))^2}}.$$

At each observation station, the wave component analysis results in a set of monthly error metrics ( $b$ ,  $E_{RMS}$ ,  $SI$ ,  $b_a$ , and  $cor$ ) that quantify the hindcast skill in reproducing the physical attributes ( $H_s$ ,  $T_p$ ,  $\bar{\theta}$  and  $\sigma$ ) of wind sea, young swell and mature swell wave systems.

By computing a variety of metrics from monthly TC and QQ analyses of the physical attributes on 1D and 2D spectral data at 7 stations for 3 hindcasts, a database of more than 10,000 independent measures of hindcast skill is generated. As will be demonstrated, this database of wave component metrics provides an extremely powerful resource for evaluating hindcast performance and identifying model strengths and deficiencies.

### 4.3 Performance Evaluation

A performance scoring method was developed to reduce the large error metric database into a small set of performance indicators for overall assessment of hindcast skill. The resulting performance scores provide a useful guide for conducting in-depth diagnostic evaluations of model behavior.

The first step in this process is to generate raw performance scores by normalizing the wave component metrics to mean quantities. These initial scores provide a basis for combining the results from multiple stations into an overall model performance for each parameter (wave height, period, direction and spread). These estimators include the RMS Error performance

$$\hat{E}_{RMS} = \left( 1 - \frac{E_{RMS}}{m_{RMS}} \right);$$

where the root-mean-square of the measurements is given by

$$m_{RMS} = \left( \frac{\sum m^2}{n} \right)^{0.5};$$

the bias performance

$$\hat{b} = \left( 1 - \frac{|b|}{m_{RMS}} \right);$$

the scatter index performance

$$\hat{SI} = (1 - SI),$$

and for directional data, the angular bias performance

$$\hat{b}_a = \left( 1 - \frac{|b_a|}{180} \right);$$

and the circular correlation performance (already normalized)

$$\hat{c}or = cor .$$

The non-dimensional performance scores range from 0 (uncorrelated) to 1 (perfect correlation) and are averaged across metrics, months and stations with contributions weighted by sample size. Hence, for a particular wave component attribute ( $H_s$ ,  $T_p$ , or  $\bar{\theta}$ ), the performance for a given month at a given station is

$$P_s = \frac{\hat{E}_{RMS} + \hat{b} + \hat{S}I}{3} \quad (\text{non-directional metrics})$$

$$P_s = \frac{\hat{b}_a + \hat{c}or}{2} \quad (\text{directional metrics})$$

with the weighted overall performance across all months and stations for each attribute

$$\bar{P} = \frac{\sum n_i P_{s_i}}{n_c} ,$$

where  $n$  denotes the total number of observations in each subset ( $i$  subscript) and for all subsets combined ( $c$  subscript).

It should be noted that directional spread ( $\sigma$ ) described earlier was dropped from the computation of all performance scores. Analysis of the data suggests that there are too few degrees of freedom in floating buoy observations to provide realistic estimates of this wave field attribute. Hence the performance scores are computed for the wave component significant wave heights ( $H_s$ ), peak periods ( $T_p$ ) and mean directions ( $\bar{\theta}$ ).

#### 4.4 Wave System Analysis

Of critical importance in evaluating hindcast performance is the determination of hindcast strengths and weaknesses leading to a diagnostic evaluation of model deficiencies. As described above, the three modeling technologies used in this study are quite similar in design, differing only in specific source term formulations and propagation schemes. Diagnostic evaluations help to identify how particular model features, such as boundary conditions, input winds, and source term formulation control the quality of the resulting hindcasts. Using the performance scores as a guide, the wave component metrics and wave system data generated by WaveMEDS provide a significant resource for conducting such evaluations.

The wave system information produced by tracking the evolving wind sea and swell components through time (Figure 2b) is used to access model performance in the

generation and evolution of wave system energy. Inputs to the analysis are the time-evolving buoy and hindcast wave system attributes  $H_s$ ,  $T_p$ , and  $\bar{\theta}$ . As described by HJ04, the total wave power  $\bar{I}$  is used to identify and select the most energetic systems for analysis. Wave system total wave power is obtained by integrating the flux of total wave energy over the duration of the wave system. Typically the 5-10 most energetic wave systems in a given monthly record are selected for enhanced analysis. For each observed wave system, time-series comparisons of hindcast wave system attributes are made.

## 5. PERFORMANCE EVALUATION RESULTS

The WaveMEDS technique was applied to all three Pacific basin wave hindcasts for the calendar year 2000. The seven deepwater NDBC and CDIP buoys depicted in Figure 1 and described in Table 2 were used as ground truth stations in the analysis. As will be demonstrated, results show that WAVEWATCH III provides a superior hindcast for the input winds, boundary conditions, and model settings employed in this study. In the following sections, a top-down reporting of results compares overall model performance for the three hindcasts and explores the spatial and seasonal variability in prediction skill for specific wave field attributes. A detailed wave system analysis is performed on the WAVEWATCH III results to identify potential deficiencies and guide future model improvements.

### 5.1 Annual Performance Summary

The annual (across-station) model performance scores for significant wave height, peak wave period and mean wave direction appear in Tables 3, 4 and 5, respectively. In each table, the results of the temporal correlations and the quantile-quantile distributions are provided for wind sea, young swell and mature swell wave components. As discussed above, the performance scores can range from 0.0 to 1.0 with 1 being a perfect match of hindcast data to observations. The combined scores (in the bottom rows) represent the weighted average (by sample size) of the performance of the three wave component classes and provide an overall measure of model skill in predicting each physical attribute (height, period and direction).

As the results indicate, all three hindcasts exhibit satisfactory performance with combined wave height scores of 0.78 to 0.88, combined wave period scores of 0.88 to 0.96, and combined wave direction scores of 0.83 to 0.91. In all cases, the QQ scores are higher than the corresponding TC scores, suggesting that the models are better skilled at representing the actual distribution of events rather than correctly matching event times. Furthermore, the wave period and wave direction scores for each model are higher than the wave height scores. Although the three models are rather close in overall performance, WAVEWATCH III consistently has the highest combined scores in each category.

The performance scores for each wave component reveal that hindcast skill varies with wave maturity. Mature swell height (Table 3) has significantly lower scores than wind

sea or young swell height in each model hindcast. As will be demonstrated, mature swell height is the most significant factor degrading model performance. For both the TC and QQ analyses, young swell height received the highest wave component score from WAM and wind sea height received the highest wave component score from WAVEWATCH III and WAVAD. This trend exhibits a surprising reversal for wave period (Table 4), as mature swell periods score higher than either wind sea or young swell periods. However the point spread in wave period across components is much less than the point spread in wave height. The wave period scores for WAM and WAVAD are quite similar for each wave component. As with wave period, the wave direction scores (Table 5) are highest for mature swell in all 3 hindcasts.

**Table 3.**  
**Significant Wave Height Performance Summary for Three Pacific Hindcasts**

Wave Height Performance Scores						
Component	Temporal Correlations			Quantile-Quantile		
	WAM	WWW III	WAVAD	WAM	WWW III	WAVAD
Wind Sea	0.79	0.88	0.83	0.82	0.92	0.88
Young Swell	0.84	0.85	0.79	0.90	0.89	0.86
Mature Swell	0.72	0.78	0.73	0.78	0.83	0.81
<b>Combined</b>	<b>0.79</b>	<b>0.84</b>	<b>0.78</b>	<b>0.83</b>	<b>0.88</b>	<b>0.85</b>

**Table 4.**  
**Peak Wave Period Performance Summary for Three Pacific Hindcasts**

Wave Period Performance Scores						
Component	Temporal Correlations			Quantile-Quantile		
	WAM	WWW III	WAVAD	WAM	WWW III	WAVAD
Wind Sea	0.87	0.92	0.89	0.91	0.96	0.94
Young Swell	0.86	0.92	0.86	0.89	0.96	0.89
Mature Swell	0.90	0.94	0.91	0.94	0.97	0.94
<b>Combined</b>	<b>0.88</b>	<b>0.93</b>	<b>0.88</b>	<b>0.91</b>	<b>0.96</b>	<b>0.92</b>

**Table 5.**  
**Mean Wave Direction Performance Summary for Three Pacific Hindcasts**

Wave Direction Performance Scores			
Component	Temporal Correlations		
	WAM	WWW III	WAVAD
Wind Sea	0.73	0.85	0.76
Young Swell	0.88	0.91	0.82
Mature Swell	0.90	0.95	0.88
<b>Combined</b>	<b>0.85</b>	<b>0.91</b>	<b>0.83</b>

## 5.2 Error Variability

Using the performance scores as a guide, the error metric details are explored to identify patterns in model deficiencies. Since mature swell height appears to be the most significant hindcast attribute responsible for lowering the combined performance scores, we focus on determining the temporal and spatial trends of the associated errors. The temporal variability in the mature swell height error metrics ( $E_{RMS}$ ,  $b$ , and  $SI$ ) at all seven ground-truth stations and for each model hindcast appears in Figure 3. The errors from a particular hindcast are organized by column and the results from a particular metric are organized by row. There is a definitive seasonal trend in mature swell height RMS error at all stations and in all three hindcasts. This trend shows that RMS errors increase during the northern hemisphere winter months (November through March), coinciding with the period of increased cyclogenesis occurring in the North Pacific. Furthermore these errors are most significant at stations 46001, 46005, and 51001 directly in the path of winter swells emanating from the North Pacific (Figure 1). It is noteworthy that in summer months, when southern swell dominates, lower wave height errors prevail.

The mature swell height bias from WAM and WAVEWATCH III (Figure 3, second row) exhibits a very similar trend to the RMS errors. In these hindcasts, mature swell height generally has a positive bias in winter months and is near zero during the remainder of the year. This trend is most distinctive in the WAVEWATCH III hindcast. In contrast, the WAVAD mature swell height biases tend to be slightly negative ( $-0.5$  m to  $0.0$  m at most stations) without a discernable seasonal trend.

At all but one station, mature swell height scatter index (Figure 3, third row) does not exhibit any specific trends across time or location, other than being slightly more variable in summer months when wave heights are lower. The exception to this is the Christmas Island station 51028, which exhibits increased  $SI$  values during northern hemisphere winter months in all three hindcasts, with particularly high values at this location ( $SI = 0.86$  in January) from WAVAD. In general, WAVEWATCH III mature swell heights exhibit lower scatter index values with the least amount of variability in time and space.

Additional details on hindcast attributes are revealed by the monthly QQ distributions prepared at each station. As a typical example, the November wave height QQ distributions at Station 51028 appear in Figure 4. The plots in this figure compare the observed and hindcast wind sea, young swell and mature swell wave height distributions computed in 99 percentile bins. The solid black line represents a perfect agreement between observation and hindcast height distributions. The WAM comparison shows that for most wave height bins, wind seas are somewhat under predicted (negative height bias) and swell is over predicted (positive height bias). As wind sea height increases, the WAM hindcast shows a much better agreement with the observations. This is supported by the HJ04 finding that WAM wind-seas exhibit a slow response to changing wind conditions and that elevated or consistently steady winds are required to match observed spectral levels. As was observed with the TC analysis, WAM mature swell heights have the largest positive bias in the QQ distributions. For WAVEWATCH III, hindcast wind sea heights show an excellent match with the observations. Swell heights above  $0.5$  m

are biased high with mature swell exhibiting the largest bias. The WAVAD QQ results depict a small positive bias in wind sea heights, and a negative bias for small swell heights switching to a very large positive bias for large mature swell heights. WAVAD young swell height distributions show generally good agreement with the observations. Although the presented QQ analyses are only representative of a single monthly record at a specific station, the trend of significantly high bias in hindcast mature swell heights prevails at all stations.

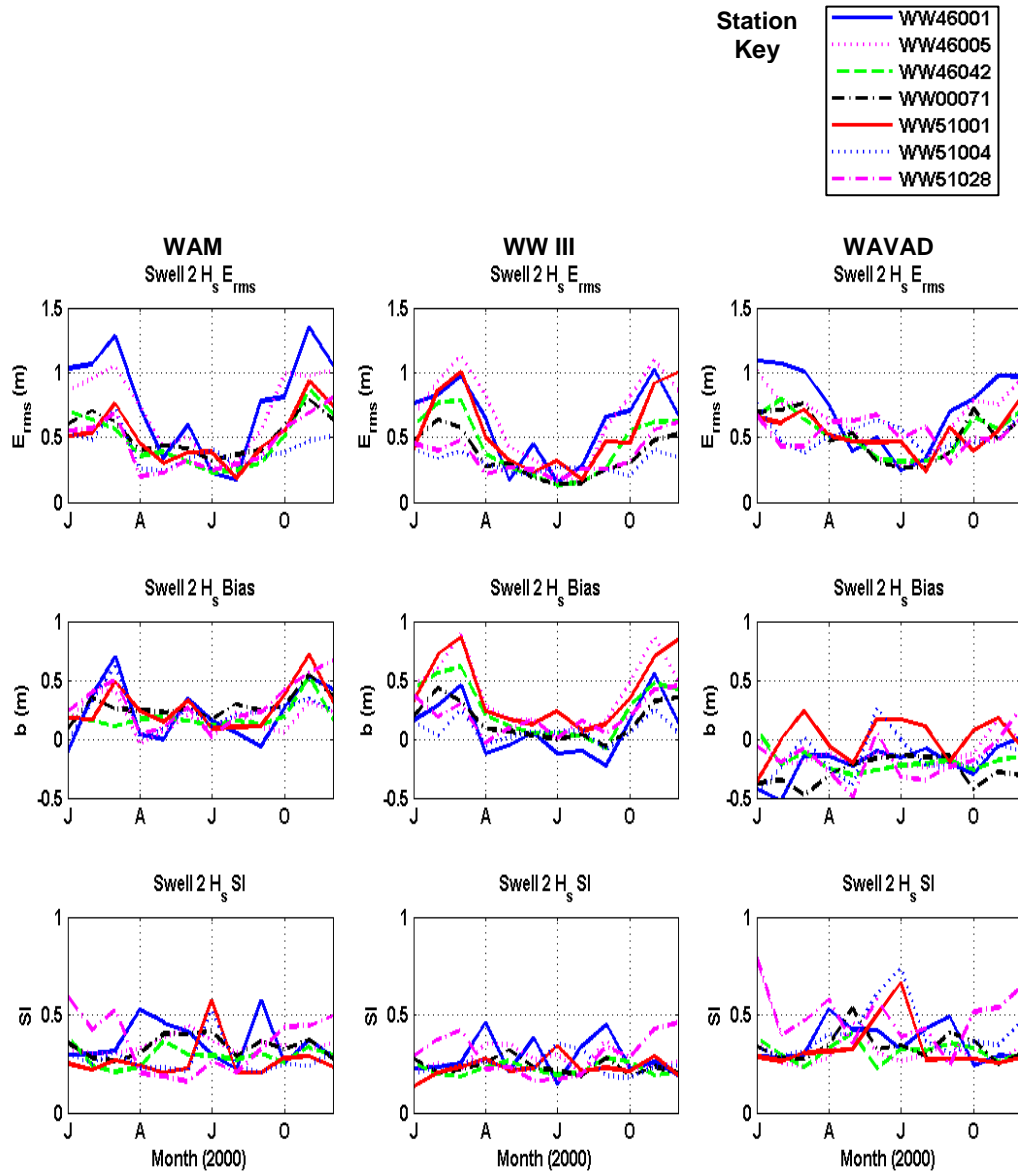


Figure 3. Seasonal variability in mature swell height errors.

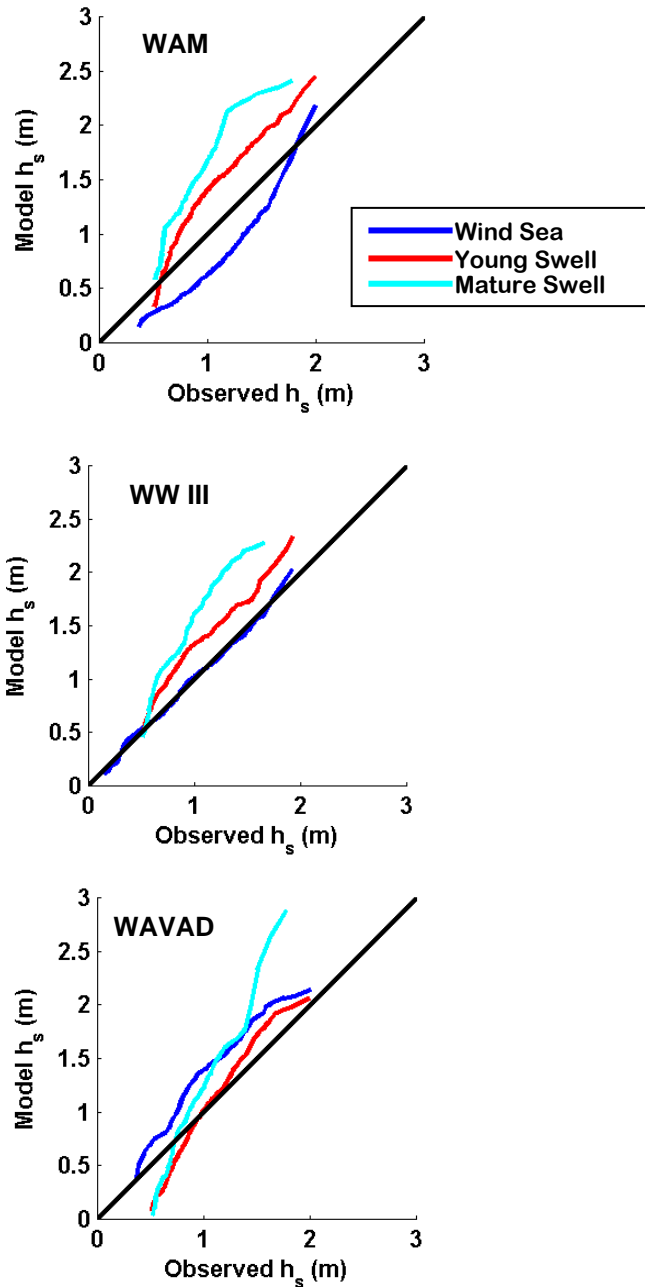


Figure 4. November wave height quantile-quantile results from Station 51028.

The results of the various hindcast performance analyses facilitated the selection of WAVEWATCH III for the on-going WIS multi-decade hindcast study. Additional results and discussion will focus primarily on this modeling technology.

### 5.3 Wave System Diagnostics

To aid in the diagnosis of WAVEWATCH III model deficiencies, a wave system approach is taken to examine the mature swell hindcast errors at directional wave station 51028. This station is located on the equator in the central Pacific and receives swell from all the major wave generation areas in the Pacific. Figure 5, reprinted here from HJ04, shows a typical November wind field with swell propagation routes from the various generation regions. HJ04 provides additional descriptions of the dynamic wave fields that exist at this station. Except for differences in the error magnitudes, the patterns of model hindcast errors at 51028 are representative of the model behavior observed at the other ground-truth stations.

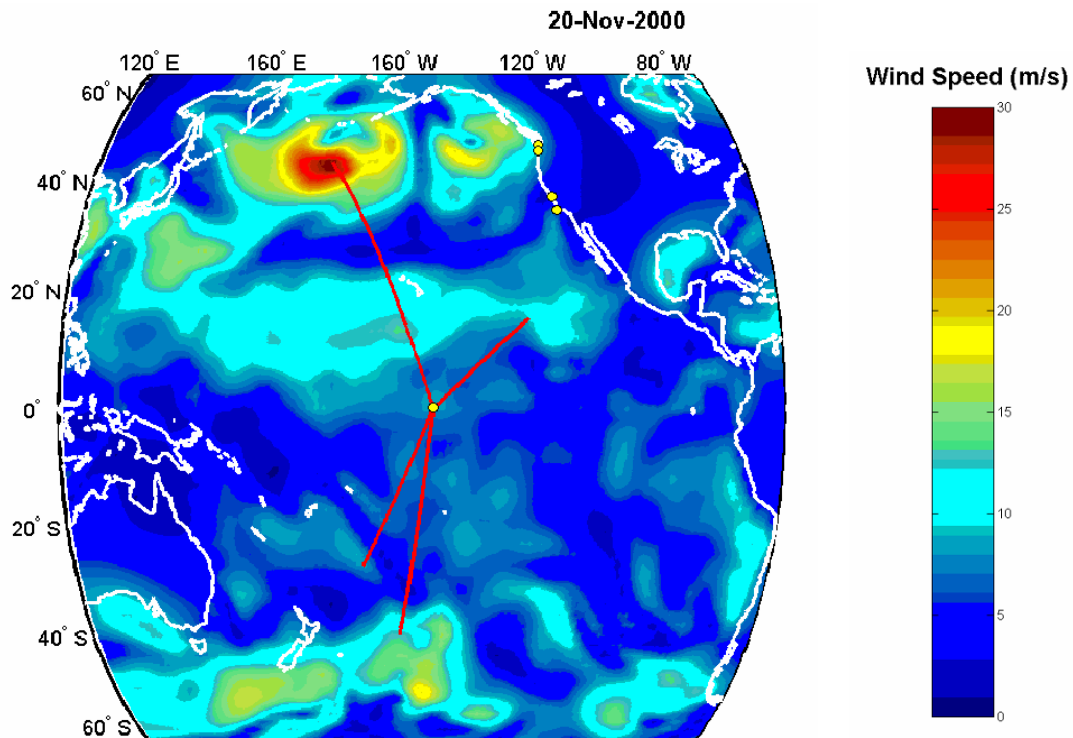


Figure 5. Example NRAQ+ wind field for 0200 GMT on 20 November 2000 showing typical wave generation routes for station 51028.

Using the total integrated wave power (see above and HJ04), the 5 most energetic wave systems at station 51028 during November 2000 were extracted from the both the WAVEWATCH III hindcast and NDBC buoy data. The resulting wave systems (A through E) are depicted in the wave vector displays of Figure 6. A striking similarity exists between the time-evolving wave systems in the hindcast and buoy records. Events A and B represent mature swell propagating north from the South Pacific, Events C and D represent mature swell propagating southeast from the North Pacific, and Event E represents young swell from the trade wind belt north of this station (Figure 5). The

wave system analysis compares the hindcast and measured events to examine differences in wave heights, periods and directions over the life cycle of each wave system. HJ04 describes a similar analysis for a previous WAM hindcast.

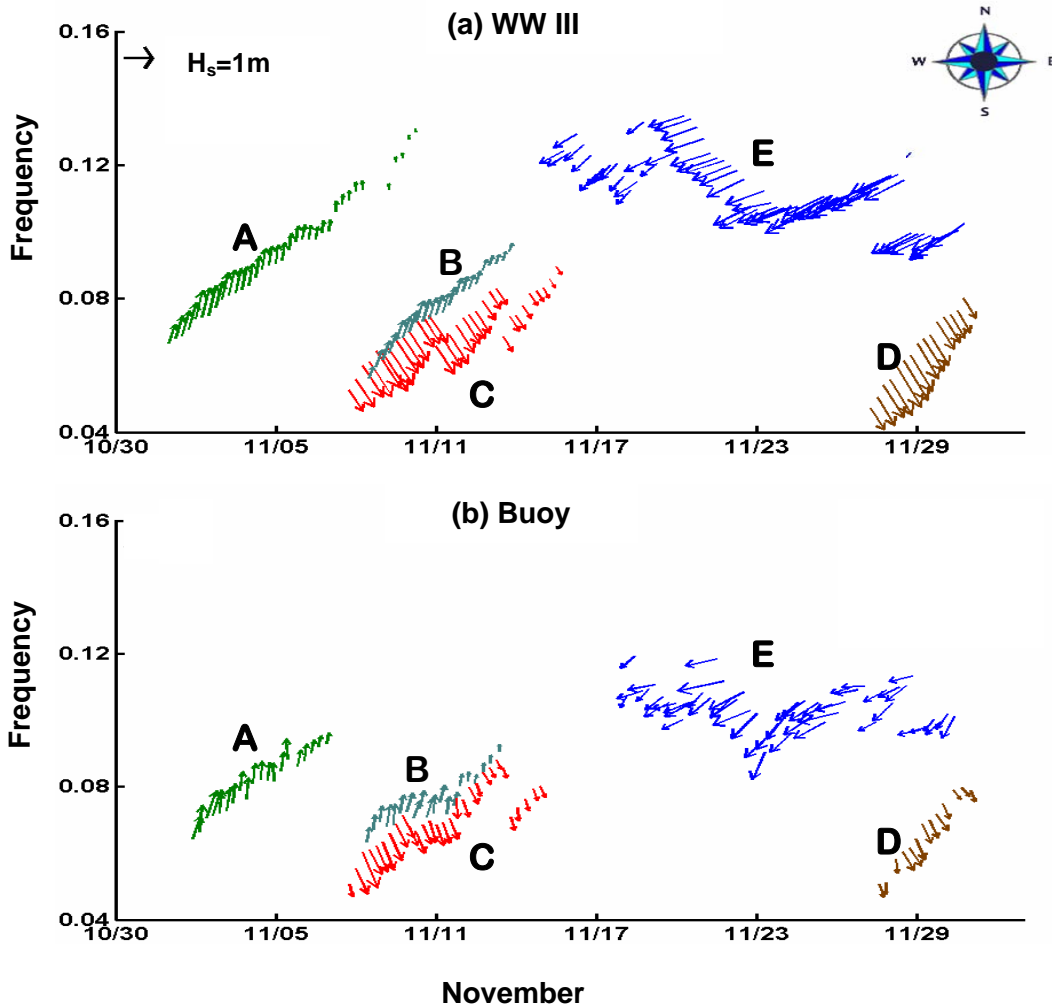


Figure 6. Vector history of most energetic wave system events during November 2000 at Station 51028: (a) WAVEWATCH III hindcast, (b) NDBC Station 51058 observations. Each vector represents wave component height, peak frequency, and direction of propagation.

Comparisons of wave system Event A as observed at station 51028 and predicted by WAVEWATCH III appear in Figure 7. Using the swell source identification methods of HP01, Figure 7a depicts the wind field at the time of generation and the great circle route this event followed to reach station 51028. The wind speed legend is identical to that depicted in Figure 5. The heights, periods and directions of this event (Figure 7b-d) are captured with minimal errors. The wave direction variability is within the 15-deg angular

resolution of the spectral data. The duration of this event is a few days longer in the hindcast record; however this is expected since very low energy components get lost in the noise of buoy data from high-energy environments. The Event B comparisons (not shown) are essentially identical to these. These results suggest that mature swell from the southern ocean are accurately represented in the WAVEWATCH III hindcast.

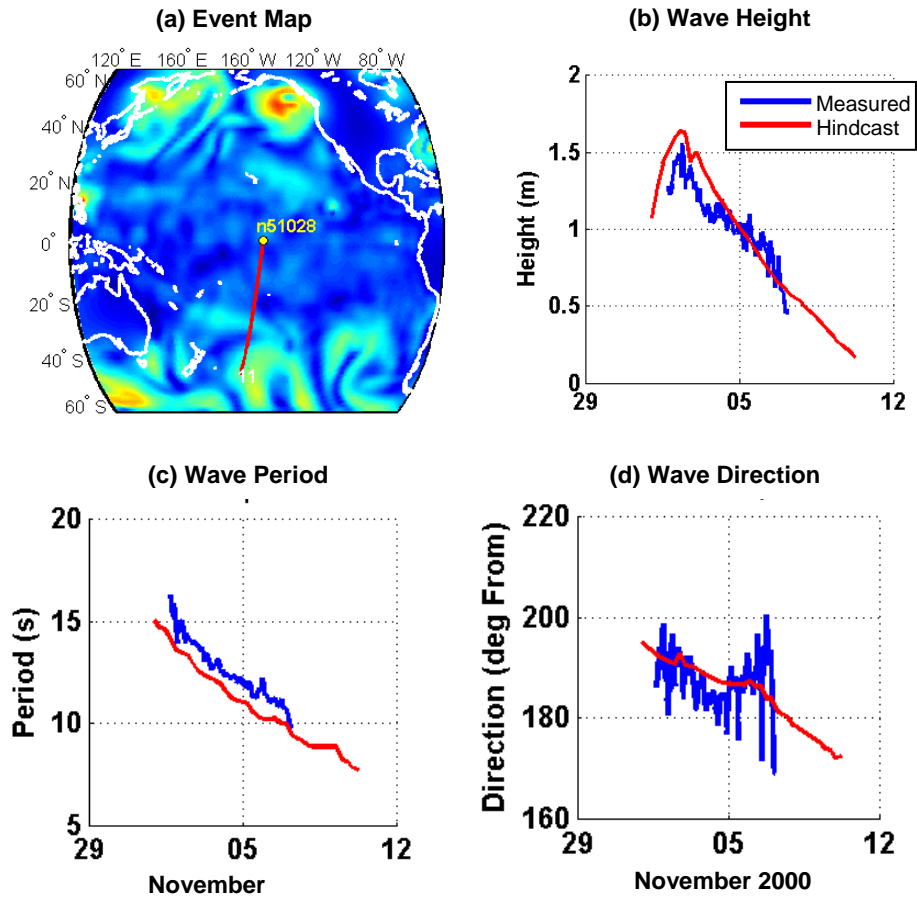


Figure 7. Station 51028 Event ‘A’ wave system analysis results for WAVEWATCH III: (a) swell propagation route, (b) wave height comparison, (c) wave period comparison, and (d) wave direction comparison.

The wave system analysis results for Event C appear in Figure 8a-d. The source for these waves was a large North Pacific low at 50 deg N Latitude. A significant wave height bias of approximately 0.5 m persists over much of this mature swell life cycle. The corresponding wave periods show a remarkable agreement between hindcast and observation. The wave direction variability is mostly within the 15-deg resolution of the data. This trend of positive height bias with period and direction agreement is also depicted by Event D (results not shown) and is typical of the WAVEWATCH III hindcast wave systems emanating from the north Pacific in winter months.

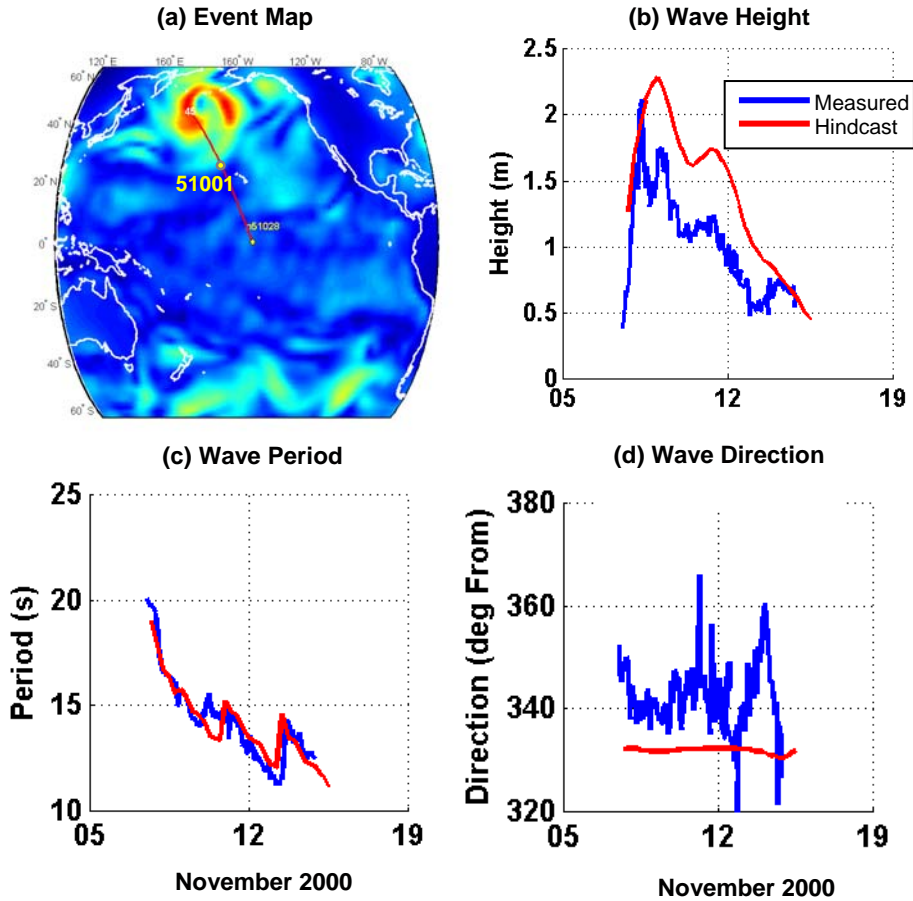


Figure 8. Station 51028 Event ‘C’ wave system analysis results for WAVEWATCH III: (a) swell propagation route, (b) wave height comparison, (c) wave period comparison, and (d) wave direction comparison.

## 6. DISCUSSION

Although the overall performance results from the Pacific hindcasts are reasonably similar, each model clearly exhibits specific strengths and weaknesses. A better understanding of these attributes can help guide model enhancements leading to future hindcast improvements. For the WAVEWATCH III year 2000 Pacific basin run, mature swell height bias appears to be the most significant hindcast limitation. We examine several possible sources of this error, including bathymetry resolution, input wind accuracy, and source term formulation.

To aid our interpretation of these results, a separate analysis was performed to compare the WAVEWATCH III hindcast total significant wave height fields to Topex/Poseidon altimeter data (Scott, 2005). Mean wave height bias was computed for year 2000 winter

months (Jan–Mar; Oct–Dec) and appears in Figure 9. This helpful display depicts the spatial extent of the wave height bias field. Note that the maximum average height biases (>0.5 m) cover a broad area of the central and eastern North Pacific Ocean, and include the areas of intensive wave generation resulting from low-pressure cyclogenesis during these months. We will refer back to this result as needed in the following discussions.

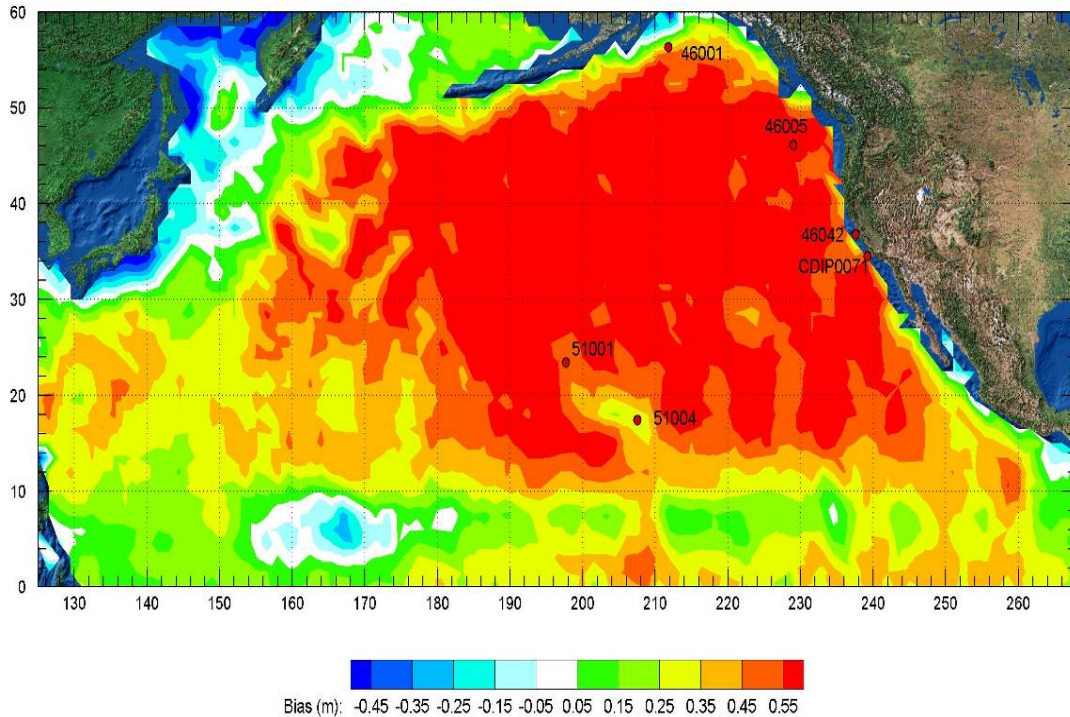


Figure 9. WAVEWATCH III total significant wave height hindcast bias for Jan-Mar, Oct-Dec 2000 derived from Topex/Poseidon altimetry data (Scott, 2005).

## 6.1 Grid Resolution

One comment received on HJ04 was that the bathymetric grid resolution was possibly too coarse, allowing excess North Pacific swell energy to ‘leak’ into the Southern Hemisphere and vice-versa. If true, this problem could account for excess mature swell height observed at the various ground-truth stations. This effect would be especially notable for swell passage west of Hawaii, as numerous small island chains, coral reefs and atolls effectively block a significant proportion of swell energy traveling between hemispheres (Hanson, 2000). As the WAVEWATCH III bathymetry grid is not of sufficient resolution to capture all of these bathymetric features, an obstruction grid is used to alleviate this problem (Tolman, 2003).

To determine if this phenomenon is responsible for the excess mature swell energy observed in the Pacific, the passage of a wave system event is examined at ground-truth

stations both above and below the Hawaiian Island chain. For this demonstration we will look at Event C from Figures 6 and 8. Note in Figure 8a that this wave system propagates southeast from a high latitude the North Pacific, through wave station 51001 northwest of Hawaii, and continues west of Hawaii down to station 51028 on the equator. As Figure 8b depicts, the hindcast swell from this event contains a swell height bias of approximately 0.5 m. The earlier passage of this same event at station 51001 is depicted in Figure 10. At this location an even greater swell height bias of approximately 1 m exists over the peak of this event. If the height bias at 51028 were a result of leakage from north of Hawaii, then one would expect to see good agreement in wave heights at station 51001. Furthermore the altimeter-derived winter height bias (Figure 9) depicts a local concentration of height bias in the deep-water region of wave generation, and hence does not support the hypothesis of energy propagating past unresolved bathymetry.

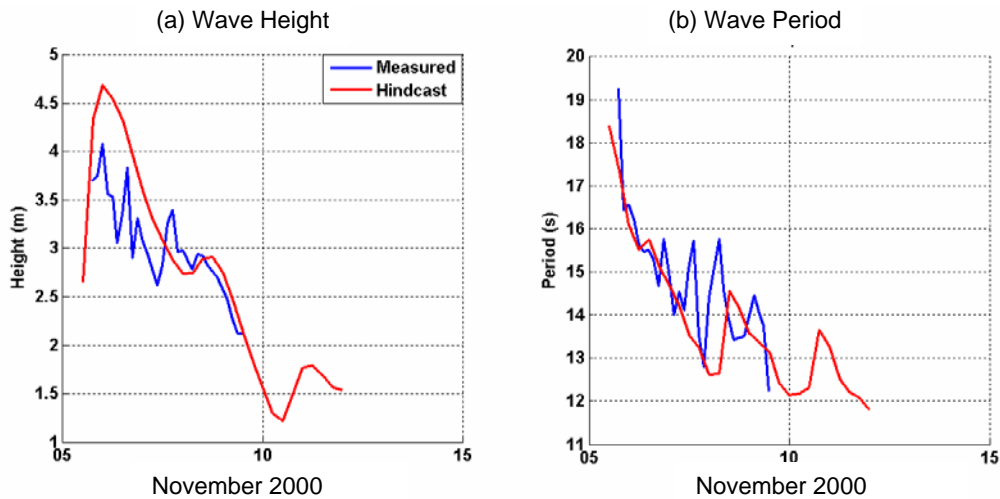


Figure 10. Station 51001 Event ‘C’ wave system analysis results for WAVEWATCH III: (a) wave height comparison, (b) wave period comparison.

## 6.2 Wind Fields

In numerical wave modeling, the quality of the output wave fields is directly related to the quality of the input winds. Although we have taken great care to secure the best possible winds for the WIS Pacific hindcast study, time and money constraints tend to dictate the ultimate quality of the final products. In this regard, a full kinematic analysis is not performed on the storm events in our WIS wind fields. This leads to the obvious question of whether our input winds are too high in the North Pacific winter region of extreme wave generation. Certainly both the WAVEWATCH III and WAM results, along with the buoy and altimeter comparisons, suggest that wind enhancement may be a significant issue contributing to mature swell height bias. It is interesting to note, however, that the WAVAD mature swell height bias is generally negative at most stations

with no discernable seasonal trend (Figure 3), and hence does not readily support the hypothesis that the North Pacific wintertime winds are elevated above realistic values.

To evaluate the impact of a more carefully constructed wind field, the marine meteorology experts at Oceanweather, Inc. conducted a full kinematic analysis on the nine most intense northern hemisphere storms occurring in March 2000. This month was selected as it includes the most extreme wind and wave event of the year – an intense low-pressure storm in the North Pacific with near hurricane-strength winds. The kinematic analysis was supported by QuickSCAT winds and included the assimilation of available buoy data. The results were blended into the March 2000 baseline NRAQ+ wind fields, resulting in a new NRAQ+K wind field for this month only. This effort generally resulted in reducing the wind speeds for these North Pacific Events. Using NRAQ+ winds to initialize the wave field, the March 2000 NRAQ+K winds were used to generate a new WAVEWATCH III hindcast. A comparison of the NRAQ+ and NRAQ+K hindcast results (total significant wave height) with buoy observations at station 51001 appears in Figure 11. Only the second half of March 2000 is depicted, to provide ample time for model adjustment to the new winds. Although the enhanced winds do yield lower wave heights during the peak events, the improvement is only a small percentage of the total bias. The rest of the stations examined exhibit a similar trend. Hence it appears that input wind magnitudes are certainly part of the swell bias problem but not the most significant contributing factor.

It is also noteworthy that the positive bias in the northern Pacific Ocean in the northern hemisphere winter has been a persistent feature of the operational WAVEWATCH III model at NCEP, based on comparisons with Jason-1, GFO and Envisat altimeter data (Tolman, unpublished data). Considering the different sources and resolutions of the wind fields involved, it is not likely that this wave model bias is a consequence of shortcomings of the wind fields.

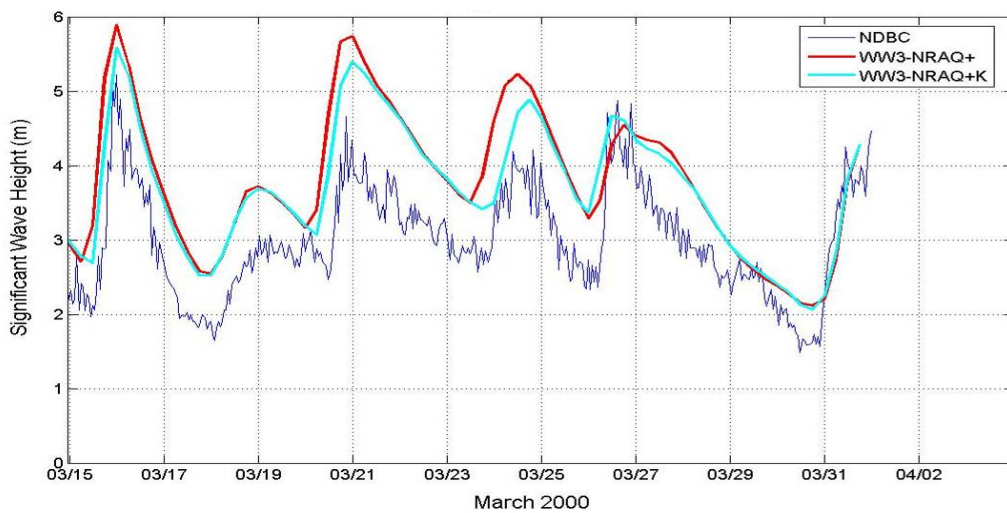


Figure 11. Comparison of WAVEWATCH III NRAQ+ and NRAQ+K hindcast wave heights with observations at station 51001.

### 6.3 Source Terms

A goal of 3G wave modeling is to capture correctly the essence of wave growth, transformation and decay while maintaining computational efficiency over large domains. Deficiencies in the physical formulation, set up, and tuning of the wind input, wave-wave interaction, and dissipation source terms can all contribute to hindcast errors. Although full treatment of this topic is far beyond the scope of this paper, a few issues are discussed here. One potential source of error is the parameterization of atmospheric drag in the wind input source term. As there have been very few direct observations of the drag coefficient  $C_D$  in extreme winds, the standard WAVEWATCH III formulation extrapolates  $C_D$  to continually increase as a function of wind speed. However recent observations suggest that  $C_D$  caps in the neighborhood of approximately  $2.5 \times 10^{-3}$  as whitecapping fully develops at wind speeds above approximately 30 m/s (Powell et al., 2003). In extreme winds, the extrapolated  $C_D$  in WAVEWATCH III could potentially lead to increased wave development and an associated wave height bias.

To test if elevated drag coefficients are contributing to the WAVEWATCH III swell height bias, an additional hindcast was made with a modified wind input source term to provide a  $C_D$  cap of  $2.5 \times 10^{-3}$ . The station 51028 performance scores for this special hindcast run exhibit only minor improvements ( $\sim 2\%$ ) over the un-capped hindcast. Results of this test run are compared with the March 2000 NRAQ+ hindcast results at station 51028 in Figure 12. The two plots depict swell component height bias as a function of hindcast wave height. Based on the direction of propagation, southern swell has been differentiated from northern swell. In both cases, the wave height bias increases somewhat linearly with wave height. The capped  $C_D$  case is nearly indistinguishable from the un-capped case and exhibits a very slight decrease in bias for some of the records. However, altimeter-derived bias for the capped  $C_D$  run show a reduction in total significant wave height of 20 to 22 cm in the central North Pacific (or roughly 5% of average wave height). Hence it appears that a capped  $C_D$  has a positive impact in the geographic area where the waves are generated. The effect on mature swell is less clear. However, the capping of  $C_D$  has a notable impact on hurricane wind wave forecasting, with reductions of maximum wave heights of up to 15% in NCEP's operational hurricane wave models (Tolman, unpublished data). Additional work in this area is warranted.

The remaining source terms (wave-wave interaction and dissipation) are likely candidates for contributing to the observed swell height bias in WAM and WAVEWATCH III. The wave-wave interaction term uses the Discrete Interaction Approximation (DIA) of Hasselmann et al., 1985. Although this computationally efficient algorithm is at the core of most 3G wave modeling, recent evidence suggests that away from the spectral peak and in multi-modal wave fields the DIA greatly under-samples the complex set of non-linear interactions taking place, leading to erroneous estimates of the spectral source function which will potentially result in spectral shapes deviating from observations (Resio, unpublished data). Furthermore, the parameterized dissipation term has largely been used as a device to tune model performance, rather than correctly capturing the physical mechanisms of wave decay. It is likely that significant gains in hindcast skill

will not be made until significant improvements are made in these source term formulations.

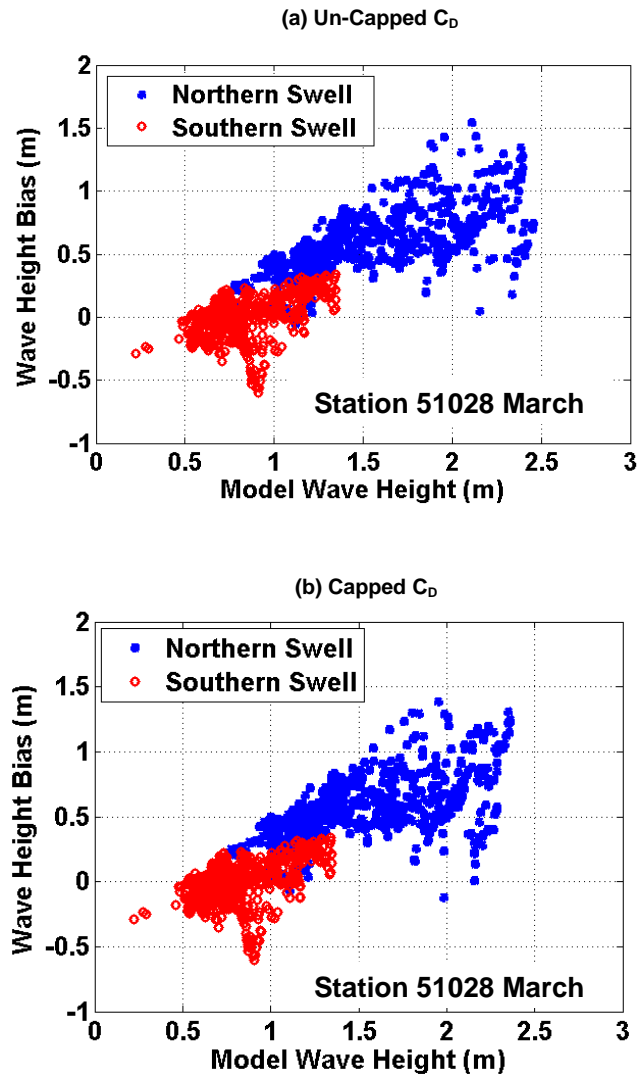


Figure 12. WAVEWATCH III hindcast results at station 51028 using (a) un-capped drag coefficient and (b) capped drag coefficient.

## 7. CONCLUSIONS

Three numerical spectral wave models were evaluated to identify the best technology for conducting a multi-decade WIS Pacific hindcast. Each technology was evaluated with identical forcing over the year 2000 with seven deep water NDBC and CDIP buoys employed as ground-truth. The wave component analysis methods contained in the Wave Model Evaluation and Diagnostics System (WaveMEDS) provided an efficient

mechanism for reducing millions of spectral values from the three hindcasts into a convenient database of monthly hindcast errors organized as a function of physical attribute (height, period and direction), wave maturity (wind sea, young swell, and mature swell) and station location. Application of a unique set of performance calculations further reduced this information into a concise set of nine overall performance scores providing a robust assessment of model prediction skill and guiding additional diagnostic evaluations.

All three models exhibited good to excellent performance in the depiction of wind sea and young swell physical attributes. A noteworthy problem area is in the prediction of mature swell in winter months, with elevated root-mean-square height errors in all three models, negative height bias in the second-generation WAVAD, and positive height bias in third-generation WAM and WAVEWATCH III hindcasts. Although the performance of all three modeling technologies was satisfactory, the WAVEWATCH III hindcast exhibited consistently higher performance scores than those from WAM and WAVAD.

The most significant factor influencing WAVEWATCH III and WAM model performance is the mature swell positive height bias during winter months. Diagnostic evaluation of these errors suggests that this problem emanates from winter swell produced in the North Pacific. This finding is also confirmed by inspection of WAVEWATCH III North Pacific hindcast bias derived from satellite altimetry. Further analysis of the data suggests that this bias does not result from energy leakage through unresolved bathymetry. Under-resolved storms in the wind fields do contribute to the height bias; however preliminary assessments suggest that extensive wind field enhancements reduce the bias by only a small percentage of the total error. A cursory examination of source term behavior shows that a cap on the atmospheric drag coefficient has a fairly positive impact on reducing wave height bias in the primary wave generation areas. The impact on mature swell is less certain. More work in this area is required. It is further suspected that the wave-wave interaction and dissipation source terms are likely contributors to swell height error, and that significant model improvements are not likely until these source terms are improved.

As a result of this analysis, WAVEWATCH III was selected for use in a new 1995-2004 Pacific Basin hindcast that is now available on the USACE WIS web page located at [http://www.frf.usace.army.mil/cgi-bin/wis/pac/pac\\_main.html](http://www.frf.usace.army.mil/cgi-bin/wis/pac/pac_main.html) .

## ACKNOWLEDGEMENTS

The authors are grateful to Elizabeth Orelup, Erin Harris, Andrew Cox, and Dr. Vince Cardone of Oceanweather, Inc. for producing the outstanding WIS wind fields; to Dr. Bob Jensen for his skillful preparation of the WAM hindcasts; to Dr. Donald Resio for several insightful suggestions to this investigation, and to Dr. Charles Long for patiently working his editorial magic on the manuscript.

## REFERENCES

- Bowers, J.A., I.D. Morton, and G.I. Mould, (2000): Directional statistics of the wind and waves, *Applied Ocean Res*, 22, 13-30.
- Cardone, V. J., R. E. Jensen, D. T. Resio, V. R. Swail, and A. T. Cox, (1996): Evaluation of contemporary ocean wave models in rare extreme events: the “Halloween Storm” of October 1991 and the “Storm of the Century” of March 1993. *J. Atmos. Oceanic Technol.*, 13, 198-230.
- Cox, A.T. and V.J. Cardone. Operational system for the prediction of tropical cyclone generated winds and waves, 6th International Workshop on Wave Hindcasting and Forecasting, November 6-10, 2000, Monterey, California.
- Cox, A. T., V. J. Cardone, and V.R. Swail, 1996: An interactive objective kinematic analysis system. *Proc. 4<sup>th</sup> International workshop on Wave Hindcasting and Forecasting*, November 6-10, 2000, Monterey, CA.
- Gunther, H. (2002): WAM Cycle 4.5, Institute for Coastal Research, GKSS Research Centre Geesthacht, 43 pp.
- Hanson, J. L., (1996): Wind sea growth and swell evolution in the Gulf of Alaska. Ph.D. Dissertation, the Johns Hopkins University, 151 pp.
- Hanson, J. L., (2000): Unpublished presentation at 6<sup>th</sup> International Workshop on Wave Hindcasting and Forecasting, November 6-10, Monterey, CA.
- Hanson, J. L., and O. M. Phillips, (2001): Automated analysis of ocean surface directional wave spectra. *J. Atmos. Oceanic Technol.*, **18**, 277-293.
- Hanson, J.L. and R. E. Jensen, (2004): Wave system diagnostics for numerical wave models, 8<sup>th</sup> International Workshop on Wave Hindcasting and Forecasting, Oahu, Hawaii, November 2004, Joint WMO/IOC Technical Commission for Oceanography and Marine Meteorology Technical Report No. 29, WMO/TD-No. 1319.
- Hasselmann, S, and K. Hasselmann, (1985): Computations and parameterizations of the nonlinear energy transfer in a gravity wave spectrum. Part I: a new method for efficient computations of the exact nonlinear transfer integral. *J. Phys. Oceanogr.*, **15**, 1369-77
- Hsu, L. Y., W. E. Rogers and J. D. Dykes, (2002): WAM performance in the Gulf of Mexico with COAMPS wind. *7<sup>th</sup> International Workshop on Wave Hindcasting and Forecasting*, Meteorological Service of Canada, 151-159.
- Kalnay, E., and Coauthors, (1996): The NCEP/NCAR 40-year reanalysis project. *Bull. Amer. Meteor. Soc.*, **77**, 437-471.
- Komen, G. J., L. Cavaleri, M. Donelan, K. Hasselmann, S. Hasselmann, and P. A. E. M. Janssen, (1994): Dynamics and Modelling of Ocean Waves. Cambridge University Press, Cambridge, UK, 560 pp.

- O'Reilly, W. C., T. H. C. Herbers, R. J. Seymour and R. T. Guza, (1996): A comparison of directional buoy and fixed platform measurements of Pacific swell. *J. Atmos. Oceanic. Technol.*, **13**, 231-238.
- Powell, M. D., P. J. Vickery, and T. A. Reinhold, (2003): Reduced drag-coefficient for high wind speeds in tropical cyclones, *Nature*, 422, 279-283.
- Resio, D. and Perrie, W., (1989): Implications of an  $f^{-4}$  equilibrium range for wind-generated waves, *J. Phys. Oceanogr.*, Vol. 19, No. 2. p. 193.
- Scott, D. (2005): Pacific Ocean Wave Information Study Validation of Wave Model Results against Satellite Altimeter Data, Draft Report, W.F. Baird and Associates, September 25, 2005.
- Tolman, H. L. and D. V. Chalikov. 1996. Source terms in a third-generation wind-wave model. *J. Phys. Oceanogr.*, 26, 2497-2518.
- Tolman, H. L. 1997. A New Global Wave Forecast System at NCEP. In: Ocean Wave Measurements and Analysis, Vol. 2, (Ed: B. L. Edge and J. M. Helmsley), ASCE, 777-786.
- Tolman, H. L. 1999: User Manual and System Documentation of WAVEWATCH-III version 1.18. Technical Note, 110 pp.
- Tolman, H. L. (2002a): User manual and system documentation of WAVEWATCH-III version 2.22. Technical Note, U.S. Department of Commerce, NOAA, NWS, NCEP, Washington, DC.
- Tolman, H. L., (2002b): The 2002 Release of WAVEWATCH III. *7<sup>th</sup> International Workshop on Wave Hindcasting and Forecasting*, Meteorological Service of Canada, 188-197.
- Tolman, H. L. (2003): Treatment of unresolved islands and sea ice in wind wave models, *Ocean Modelling*, 5, 219-231.
- Tracy, B.A., (2002): Directional characteristics of the 1990-1999 Wave Information Studies Gulf of Mexico hindcast, *7<sup>th</sup> International Workshop on Wave Hindcasting and Forecasting*, October 21-25, Banff, Alberta, Canada.
- Tracy, B. A and A. Cialone, (2004): Comparison of Gulf of Mexico Wave Information Studies (WIS) 2-G hindcast with 3-G hindcasting, *8<sup>th</sup> International Workshop on Wave Hindcasting and Forecasting*, Oahu, Hawaii, November 2004, Joint WMO/IOC Technical Commission for Oceanography and Marine Meteorology Technical Report No. 29, WMO/TD-No. 1319.